Frequency Estimation by Interpolation of Two Fourier Coefficients: Cramér-Rao Bound and Maximum Likelihood Solution

Antonio Alberto D'Amico, Michele Morelli, *Senior Member, IEEE*, and Marco Moretti, *Member, IEEE*

***Abstract*— Sinusoidal frequency estimation in the presence of white Gaussian noise plays a major role in many engineering fields. Significant research in this area has been devoted to the fine tuning stage, where the discrete Fourier transform (DFT) coefficients of the observation data are interpolated to acquire the residual frequency error ε. Iterative interpolation schemes have recently been designed by employing two q-shifted spectral lines symmetrically placed around the DFT peak, and the impact of q on the estimation accuracy has been theoretically assessed. Such analysis, however, is available only for some specific algorithms and is mostly conducted under the assumption of a vanishingly small frequency error, which makes it inappropriate for the first stage of any iterative process. In this work, further investigation on DFT interpolation is carried out to examine some issues that are still open. We start by evaluating the Cramér-Rao bound (CRB) for frequency recovery by interpolation of two q-shifted spectral lines and assess its dependence on ε and q. Such a bound is of primary importance to check whether existing schemes can provide efficient estimates at *any* iteration or not. After determining the optimum value of q for a given ε, we eventually derive the maximum likelihood (ML) DFT interpolator. Since the latter exhibits the best performance at any step of the iteration process, it might attain the desired accuracy just at the end of the first iteration, which is especially advantageous in terms of computational load and processing time.**

***Index Terms*— Frequency estimation, DFT interpolation, Cramér-Rao bound, parameter estimation.**

I. Introduction

ESTIMATING the frequency of a complex sinusoid corrupted by white Gaussian noise (WGN) is a fundamental problem that appears in many areas of science and technology, such as wireless communications [1], biomedical applications, power grid systems [2] and radar signal processing [3]. The maximum likelihood (ML) solution, along with the relevant Cramér-Rao bound (CRB), was originally derived in [4] and is given by the argument of the periodogram maximizer. Since the numerical maximization of the periodogram is computationally demanding, one common approach for frequency recovery relies on a two-step procedure consisting of a coarse search followed by a fine tuning step. The coarse estimation stage evaluates the DFT of the input data sequence and provides an estimate of the integer frequency offset (IFO) by locating the index of the bin with the highest magnitude. Interpolation techniques are subsequently used in the fine tuning stage in order to determine the residual fractional frequency offset (FFO) through a local search conducted in the neighborhood of the maximum bin. The total computational cost of this approach is mainly involved in the DFT evaluation and amounts to $\mathcal{O}(N \log_2 N)$, where N is the length of the data record. Alternative schemes for frequency recovery employ the sample autocorrelation function of the observed data [5], [6], [7]. Compared to DFT-based methods, they dispense from any grid-search at the price of an increased processing load, which is in the order of $\mathcal{O}(N^2)$. Another class of popular estimation techniques employed in spectral analysis is represented by subspace-based methods, including MUSIC (MUltiple SIgnal Classification) [8] or ESPRIT (Estimation of Signal Parameters via Rotational Invariance Techniques) [9]. These algorithms are typically used to resolve closely separated spectral lines through an eigenvalue or a singular value decomposition. However, since the required computational cost is as high as $\mathcal{O}(N^3)$, their adoption is not recommended in the presence of a single sinusoidal signal. As an alternative to MUSIC or ESPRIT, the atomic norm minimization principle has recently been suggested for super resolution spectral line estimation [10]. Theoretical analysis indicates that the accuracy of this approach matches the CRB up to a logarithmic factor. Due to their reduced complexity, in this work we concentrate on the class of DFT-based frequency estimators, which represent the preferred choice for estimating the parameters of a single sinusoid embedded in WGN. In particular, we assume that the initial coarse search has been successfully completed and turn our attention to the DFT interpolation stage.

Numerous efforts have been made in the past to achieve fast and accurate frequency recovery through DFT interpolation. Existing solutions can be roughly divided into two categories: direct methods [11], [12], [13], [14], [15], [16], [17], [18] and iterative schemes [19], [20], [21], [22], [23], [24]. The former operate by reprocessing the maximum DFT coefficient and its neighbours that are available from the coarse search stage. Hence, they provide the FFO estimate with negligible additional cost, which makes them particularly attractive in many situations. In particular, the methods suggested

Manuscript received 22 January 2022; revised 27 May 2022 and 10 August 2022; accepted 11 August 2022. Date of publication 22 August 2022; date of current version 18 October 2022. This work was supported by the Italian Ministry of Education and Research (MIUR) in the Framework of the Cross Laboratory Project (Departments of Excellence). The associate editor coordinating the review of this article and approving it for publication was S. Bhashyam. *(Corresponding author: Antonio Alberto D'Amico.)*

The authors are with the Dipartimento di Ingegneria dell'Informazione, University of Pisa, 56122 Pisa, Italy (e-mail: antonio.damico@unipi.it; michele.morelli@unipi.it; marco.moretti@unipi.it).

Digital Object Identifier 10.1109/TCOMM.2022.3200679

This work is licensed under a Creative Commons Attribution 4.0 License. For more information, see https://creativecommons.org/licenses/by/4.0/

in [11], [12], [13], [14], and [15] employ three DFT samples, while Macleod in [16] modified the interpolator of [12] and also proposed a five-sample interpolator. Schemes that can utilize an arbitrary number of DFT coefficients are presented in [17] and [18]. A common drawback of direct interpolation methods is that their accuracy is non-uniform over the FFO search range and cannot attain the classical CRB (CCRB) reported in [4]. Indeed, theoretical analysis conducted in [18] indicates that the ultimate accuracy achievable by direct schemes is largely influenced by the FFO value and the worst case occurs for a signal frequency coinciding with one of the DFT bins. In such a case, the loss incurred with respect to the CCRB amounts to $\pi^2/6 \approx 1.645$ when three DFT samples are used in the fine tuning stage.

In order to achieve close to uniform performance, the concept of iterative interpolation must be resorted to. Estimators obeying to such a criterion operate in a recursive fashion, where the residual FFO obtained at an earlier iteration is removed from the input signal and the interpolation procedure is subsequently reapplied to the compensated data. This way, the FFO is progressively reduced until convergence. Compared to direct interpolation methods, iterative schemes exhibit improved accuracy at the price of an increased computational load. The reason is that, at each new iteration, they need the evaluation of two auxiliary spectral lines symmetrically shifted around the peak DFT coefficient. The shift value depends on the specific algorithm. For example, the frequency estimators presented by Aboutanios and Mulgrew (named AME1 and AME2) in [19] apply a shift of $\pm 0.5\Delta f$, where Δf is the distance between two adjacent DFT bins. Using the fixed-point theorem, it is shown that both schemes converge after two iterations, thereby requiring four auxiliary DFT samples to complete the fine tuning stage. Methods to reduce the processing load without sacrificing the system performance are reported in [20], [21], and [22]. More recently, Fan and Qi [23] have proposed an iterative scheme (denoted as FQE) based on interpolation of three DFT coefficients, namely the central DFT peak and two auxiliary spectral lines with arbitrary shifts of $\pm q\Delta f$. They also assess the impact of q on the estimation accuracy and the best performance is found to occur when q approaches zero. A similar investigation is executed in [24], where two iterative estimators named QSE and HAQSE are derived using only two q-shifted DFT coefficients, thereby excluding the central DFT peak from the estimation process. In such a case, the optimum value of q is found to depend on the number N of observed data, and approaches zero as N grows large. A refined region for q is derived in [25] to ensure convergence of QSE even in the presence of small data records.

Theoretical investigation reported in [23] and [24] indicates that, upon convergence, the accuracy of FQE, QSE and HAQSE asymptotically attains the CCRB when the DFT shift q is properly designed. Since these algorithms are iterative in nature, the residual FFO is expected to become very small after a few iterations. Hence, in order to predict the system performance at the end of the iterative process, theoretical analysis is conducted in [24] under the assumption that the residual frequency error is close to zero. Clearly, such analysis cannot be applied at the beginning of the iterative process, when the initial FFO value can in principle be as large as $\pm 0.5\Delta f$. This means that the estimation accuracy after the first iteration might substantially deviate from the CCRB and might be non uniform over the entire frequency range. We also emphasize that, so far, the optimum value of q has been devised only for the specific algorithms presented in [23] and [24], while a more general criterion for the design of this parameter is still unavailable. Hence, assuming that two auxiliary DFT coefficients with arbitrary shifts $\pm q\Delta f$ are involved in the fine tuning stage, the following issues remain open to question and deserve further investigation:

1) What is the *best* accuracy that can be achieved in the estimation of the residual frequency error for given values of q and ε?
2) What is the optimum value of q leading to the minimum estimation variance for a given ε?
3) What is the optimum estimator based on two q-shifted interpolated DFT coefficients that exhibits the best accuracy at *any* iteration?

This work provides answers to all the aforementioned issues. The framework is the same adopted in [24], where two spectral lines symmetrically placed around the DFT central peak are employed for fine frequency tuning. In particular, the first issue is examined by evaluating the Cramér-Rao bound for the considered estimation problem. As we shall see, such a bound is a function of q and is generally higher than the CCRB, meaning that the latter cannot be attained at the first iteration. Based on the results reported in [23] and [24], the optimum value of q that minimizes the bound, say $q_{\rm opt}$, is likely to approach zero when the residual frequency error is vanishingly small. However, higher values of $q_{\rm opt}$ can reasonably be expected when the FFO deviates from zero, as in such a case the suspicion arises that optimum interpolation requires the FFO to lay between the auxiliary spectral lines. The second issue of our study aims at checking whether such a conjecture is true or not. The answer is found by looking for the minimum of the novel bound with respect to q and assessing its dependence on the residual frequency error. The third issue is eventually explored by deriving the ML interpolator that operates on two q-shifted DFT coefficients. As is known, the ML rule provides a scheme that is asymptotically efficient so that, at any iteration, it exhibits the best accuracy over the class of unbiased estimators. This results into some potential advantages with respect to competing schemes, such as increased robustness and a reduced number of iterations to achieve the desired estimation accuracy. For example, the ML solution could provide satisfactory performance just at the end of the first iteration, thereby dispensing from further iterations as requested by FQE, QSE and HAQSE. In such a case, the fine tuning stage would benefit from some computational saving and reduced processing time, which are highly desirable in fast real-time applications.

The remainder of the paper is organized as follows. Next section provides the system model and some basic notation. In Sect III, we present CRB analysis for q-shifted DFT interpolation and determine the value of q that minimizes the bound for a specified frequency error. The ML interpolator is

derived in Sect. IV, where an efficient method to maximize the ML metric is also introduced. Simulation results are illustrated in Sect. V, while some conclusions are drawn in Sect VI.

Notation: Matrices and vectors are denoted by boldface letters, with $\mathbf{A}^{-1}$ being the inverse of a matrix $\mathbf{A}$. We use $\mathrm{E}\{\cdot\}$, $(\cdot)^*$, $(\cdot)^T$ and $(\cdot)^H$ for expectation, complex conjugation, transposition and Hermitian transposition, respectively. The notation $\mathrm{Re}\{\cdot\}$ stands for the real part of a complex-valued quantity, $\mathrm{Im}\{\cdot\}$ for the imaginary part and $|\cdot|$ for its modulus. Finally, we denote by $\tilde{\lambda}$ a trial value of an unknown parameter λ, while $\hat{\lambda}$ is the corresponding estimate.

II. System Model

The mathematical model of a discrete-time complex exponential signal embedded in additive noise is given by

$$x(n) = Ae^{j(2\pi n\nu+\theta)} + w(n) \quad n = 0, 1, \ldots, N-1 \tag{1}$$

where N is the length of the data record, while $\{A, \nu, \theta\}$ specify the amplitude, the frequency and the initial phase of the signal component, respectively. The noise contribution is represented by $\{w(n)\}$, which is modeled as a circularly symmetric additive white Gaussian process with power $\sigma^2 = \mathrm{E}\{|w(n)|^2\}$. Accordingly, the signal-to-noise ratio (SNR) is defined as A^2/σ^2. Without any loss of generality, we can rewrite the incoming data as

$$x(n) = Ae^{j2\pi[n-(N-1)/2]\nu}e^{j\varphi} + w(n) \quad n = 0, 1, \ldots, N-1 \tag{2}$$

where $\varphi = \theta + \pi(N-1)\nu$ is the phase value at the centre of the observation window. Such a reformulation turns out to be useful to simplify the subsequent analysis.

The ML estimate of ν in the presence of the nuisance parameters $\{A, \varphi\}$ was originally derived in [4] and is given by the value $\hat{\nu}_{ML}$ that maximizes the periodogram of the input data. Such a maximization is computationally demanding as it requires a grid-search over the set spanned by the continuous variable ν. A more practical approach is based on a two-stage procedure, according to which the frequency ν is divided into an integer part k_p plus a residual FFO ε, yielding

$$\nu = \frac{k_p + \varepsilon}{N} \tag{3}$$

with $k_p = 0, 1, \ldots, N-1$ and $\varepsilon \in [-0.5, 0.5)$. In the first stage (coarse search), an estimate of k_p is found by computing the $N-$point DFT of the incoming data and picking the coefficient with the highest magnitude, i.e.,

$$\hat{k}_p = \arg\max_k |X(k)| \tag{4}$$

with

$$X(k) = \sum_{n=0}^{N-1} x(n)e^{-j2\pi nk/N} \quad k = 0, 1, \ldots, N-1. \tag{5}$$

In the second stage (fine search), the residual error ε is recovered by interpolating between the DFT peak sample $X(\hat{k}_p)$ and a few neighboring spectral lines. While direct interpolation methods employ a subset of the DFT coefficients $\{X(k)\}$ already available from the coarse search, iterative schemes make use of two additional spectral lines with fractional shifts $\pm q$ from the central DFT peak. For example, the value $q = 0.5$ is chosen in [19], while the impact of q on the system performance is investigated in [23] and [24]. In the latter works, the authors derive the optimum value of q for FQE and QSE and show that, after some iterations, the estimation accuracy attains the classical CRB for FFO recovery, which is expressed by [4]

$$\mathrm{CCRB} = \frac{3\sigma^2 N}{2\pi^2 A^2 (N^2-1)}. \tag{6}$$

Their analysis, however, only applies to FQE and QSE, so that there is no guarantee that the values of q found in [23] and [24] can provide the best accuracy within the class of q-shifted DFT interpolators. Furthermore, the performance of QSE is theoretically assessed in [24] under the assumption that the residual frequency error is close to zero, which occurs only after completing at least one iteration. Hence, the question arises as to whether some performance improvement is possible or not during the first step of the iterative process, when the FFO can take any value in the interval $[-0.5, 0.5)$. Our study provides a convincing answer to such a question. Specifically, we use CRB analysis to evaluate the *ultimate* accuracy achievable in the estimation of ε when two q-shifted spectral lines are available as observation data. The impact of q and ε on the bound is also investigated in order to check whether values of q other than those suggested in [23] and [24] can provide improved accuracy at the first iteration. We eventually derive the optimum ML scheme for q-shifted DFT interpolation, and assess its performance in terms of estimation accuracy and processing load.

III. Cramér-Rao Bound for q-Shifted DFT Interpolation

A. Analytical Model of the Auxiliary Spectral Lines

We assume that the coarse search stage has been successfully completed, which amounts to putting $\hat{k}_p = k_p$. Hence, the q-shifted DFT coefficients employed for FFO recovery are computed as

$$X_r = \sum_{n=0}^{N-1} x(n)e^{-j2\pi[n-(N-1)/2](k_p+r)/N} \tag{7}$$

with $r = \pm q$. It is worth recalling that the assumption $\hat{k}_p = k_p$ is reasonable only in the medium or high SNR regime. Indeed, at low SNR values the periodogram may be so distorted by noise that its maximum is occasionally placed far removed from k_p. In such a case, the frequency estimate is affected by large errors, known as *outliers* [4]. The SNR below which outliers start to occur is known as the *threshold* of the estimator and depends on the length of the data record. In [26], it is found that the SNR threshold is close to 0 dB when $N = 64$ and approximately reduces by 2.75 dB whenever N is doubled. These results provide useful guidelines for the selection of N, given that in a correctly designed system the estimator should operate well above its SNR threshold.

Substituting (2) into (7) and bearing in mind (3), yields

$$X_r = (C_R + jC_I)NS_r + W_r \tag{8}$$

where C_R and C_I are the real and imaginary parts of $Ae^{j\varphi}$, respectively, and we have defined the quantities

$$S_r = \frac{1}{N}\sum_{n=0}^{N-1} e^{j2\pi[n-(N-1)/2](\varepsilon-r)/N} \tag{9}$$

and

$$W_r = \sum_{n=0}^{N-1} w(n)e^{-j2\pi[n-(N-1)/2](k_p+r)/N}. \tag{10}$$

Letting

$$f_N(x) = \frac{\sin(\pi x)}{N\sin(\pi x/N)} \tag{11}$$

we can rewrite S_r as

$$S_r = f_N(\varepsilon - r) \tag{12}$$

while W_r is a zero-mean Gaussian random variable. We collect the two auxiliary DFT coefficients into a vector $\mathbf{X} = [X_{-q}, X_q]^T$ and rewrite (8) as

$$\mathbf{X} = (C_R + jC_I)N\mathbf{S} + \mathbf{W} \tag{13}$$

where $\mathbf{S} = [S_{-q}, S_q]^T$ and $\mathbf{W} = [W_{-q}, W_q]^T$. In Appendix A, we show that the noise terms $W_{\pm q}$ have equal power $\mathrm{E}\{|W_{\pm q}|^2\} = N\sigma^2$ and covariance $\mathrm{E}\{W_{-q}W_q^*\} = N\sigma^2 f_N(2q)$. Hence, letting $\gamma = f_N(2q)$, it turns out that $\mathbf{W}$ is Gaussian distributed with zero mean and covariance matrix

$$\mathbf{C}_W = N\sigma^2\begin{bmatrix} 1 & \gamma \\ \gamma & 1 \end{bmatrix}. \tag{14}$$

B. CRB Evaluation

Our goal is to find the CRB for the estimation of ε based on the observation vector $\mathbf{X}$. The presence of the nuisance parameters $\{C_R, C_I\}$ requires the evaluation of the Fisher information matrix (FIM) for the set $\boldsymbol{\xi} = \{C_R, C_I, \varepsilon\}$. Observing that $\mathbf{X}$ is Gaussian distributed with mean

$$\boldsymbol{\mu} = (C_R + jC_I)N\begin{bmatrix} f_N(\varepsilon+q) \\ f_N(\varepsilon-q) \end{bmatrix} \tag{15}$$

and covariance matrix $\mathbf{C}_W$, the entries of the FIM are given by [27]

$$[\mathbf{F}]_{i,j} = 2\mathrm{Re}\left\{\frac{\partial\boldsymbol{\mu}^H}{\partial\xi_i}\mathbf{C}_W^{-1}\frac{\partial\boldsymbol{\mu}}{\partial\xi_j}\right\} \quad 1 \le i,j \le 3 \tag{16}$$

where we have used the notation $\xi_1 = C_R, \xi_2 = C_I$ and $\xi_3 = \varepsilon$. The derivatives of $\boldsymbol{\mu}$ with respect to the unknown parameters are easily computed from (15) as

$$\frac{\partial\boldsymbol{\mu}}{\partial\xi_1} = N\mathbf{S}, \quad \frac{\partial\boldsymbol{\mu}}{\partial\xi_2} = jN\mathbf{S}, \quad \frac{\partial\boldsymbol{\mu}}{\partial\xi_3} = NC\boldsymbol{\alpha} \tag{17}$$

where $\boldsymbol{\alpha} = [\alpha_{-q}, \alpha_q]^T$ has entries

$$\alpha_r = f_N'(\varepsilon - r) \quad r = \pm q \tag{18}$$

and $f_N'(x)$ is the derivative of $f_N(x)$ with respect to x. Substituting the results (17) into (16) yields the FIM

$$\mathbf{F} = \frac{2N}{\sigma^2(1-\gamma^2)}\begin{bmatrix} \mathbf{S}^T\mathbf{D}\mathbf{S} & 0 & C_R\mathbf{S}^T\mathbf{D}\boldsymbol{\alpha} \\ 0 & \mathbf{S}^T\mathbf{D}\mathbf{S} & C_I\mathbf{S}^T\mathbf{D}\boldsymbol{\alpha} \\ C_R\mathbf{S}^T\mathbf{D}\boldsymbol{\alpha} & C_I\mathbf{S}^T\mathbf{D}\boldsymbol{\alpha} & |C|^2\boldsymbol{\alpha}^T\mathbf{D}\boldsymbol{\alpha} \end{bmatrix} \tag{19}$$

with

$$\mathbf{D} = \begin{bmatrix} 1 & -\gamma \\ -\gamma & 1 \end{bmatrix} \tag{20}$$

and

$$\begin{aligned}\mathbf{S}^T\mathbf{D}\mathbf{S} &= [f_N(\varepsilon+q) - f_N(\varepsilon-q)]^2 \\ &\quad + 2(1-\gamma)f_N(\varepsilon+q)f_N(\varepsilon-q) \qquad (21)\\ \boldsymbol{\alpha}^T\mathbf{D}\boldsymbol{\alpha} &= [f_N'(\varepsilon+q) - f_N'(\varepsilon-q)]^2 \\ &\quad + 2(1-\gamma)f_N'(\varepsilon+q)f_N'(\varepsilon-q) \qquad (22)\\ \mathbf{S}^T\mathbf{D}\boldsymbol{\alpha} &= [f_N(\varepsilon+q) - f_N(\varepsilon-q)][f_N'(\varepsilon+q) - f_N'(\varepsilon-q)] \\ &\quad + (1-\gamma)[f_N(\varepsilon-q)f_N'(\varepsilon+q) \\ &\quad + f_N(\varepsilon+q)f_N'(\varepsilon-q)]. \qquad (23)\end{aligned}$$

The CRB for the estimation of ε is $[\mathbf{F}^{-1}]_{3,3}$. This is obtained from (19) as

$$\mathrm{CRB}(\varepsilon, q) = \frac{\sigma^2(1-\gamma^2)}{2NA^2}\cdot\frac{\mathbf{S}^T\mathbf{D}\mathbf{S}}{(\mathbf{S}^\mathbf{T}\mathbf{D}\mathbf{S})(\boldsymbol{\alpha}^T\mathbf{D}\boldsymbol{\alpha}) - (\mathbf{S}^T\,\mathbf{D}\boldsymbol{\alpha})^2} \tag{24}$$

where the notation $\mathrm{CRB}(\varepsilon, q)$ is used to explicitly indicate the dependence of the bound on ε and q. It is interesting to assess the loss incurred in the estimation of ε when the samples $X_{\pm q}$ are used as observation variables instead of the entire set of N DFT coefficients. The loss is quantified by the ratio between $\mathrm{CRB}(\varepsilon, q)$ and the CCRB reported in (6)

$$L(\varepsilon, q) = \frac{\mathrm{CRB}(\varepsilon, q)}{\mathrm{CCRB}} \tag{25}$$

and is expressed by

$$L(\varepsilon, q) = \frac{(1-\gamma^2)(N^2-1)\pi^2}{3N^2}\cdot\frac{\mathbf{S}^T\mathbf{D}\mathbf{S}}{(\mathbf{S}^\mathbf{T}\mathbf{D}\mathbf{S})(\boldsymbol{\alpha}^T\mathbf{D}\boldsymbol{\alpha}) - (\mathbf{S}^T\mathbf{D}\boldsymbol{\alpha})^2}. \tag{26}$$

Fig. 1 illustrates $L(\varepsilon, q)$ as a function of q for some values of ε and $N = 64$. As is seen, the loss monotonically increases with q and attains its global minimum when q approaches zero, irrespective of the FFO value. This means that, for any value of ε, the best accuracy is achieved when the q-shifted spectral lines tend to collapse onto the central DFT peak $X(\hat{k}_p)$. Such a result is very surprising and somewhat unexpected. Indeed, in the extreme case in which q is exactly set to zero, only $X(\hat{k}_p)$ would remain available for the fine tuning stage, which precludes the possibility of executing any interpolation procedure. In such a situation, the FFO can no longer be retrieved and the bound is expected to diverge to infinity, in contrast to what is observed in Fig. 1. The fact that the best accuracy is achieved when q approaches zero

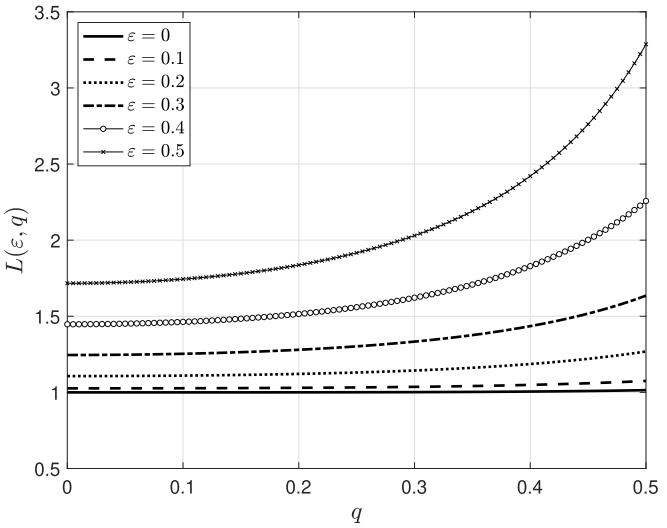

Fig. 1. $L(\varepsilon, q)$ vs. q for some values of ε and $N = 64$.

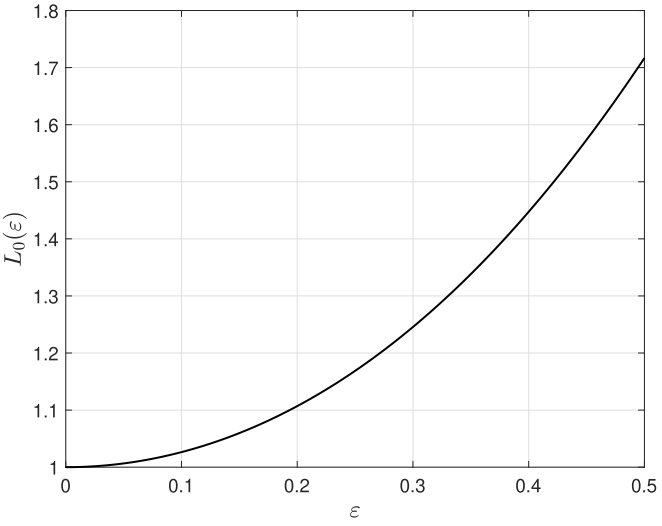

Fig. 2. $L_0(\varepsilon)$ vs. ε for $N = 64$.

was also found in [24] in the specific case $\varepsilon = 0$. What makes the curves in Fig. 1 counter-intuitive is that they predict the same behaviour even when ε is close to ± 0.5, while in the latter scenario one might reasonably suspect that the best interpolation accuracy is obtained when ε lies in the interval $[-q, q]$.

C. CRB Analysis for $q \to 0$

In light of the results shown in Fig. 1, it is useful to find an expression of $\mathrm{CRB}(\varepsilon, q)$ when q approaches zero. This quantity is denoted by

$$\mathrm{CRB}_0(\varepsilon) = \lim_{q \to 0} \mathrm{CRB}(\varepsilon, q) \tag{27}$$

and is evaluated in Appendix B using standard Taylor series analysis, yielding

$$\mathrm{CRB}_0(\varepsilon) = \frac{\sigma^2}{6N^3A^2} \cdot \frac{3N^2 f_N'^2(\varepsilon) + \pi^2(N^2-1) f_N^2(\varepsilon)}{\left[f_N(\varepsilon) f_N''(\varepsilon) - f_N'^2(\varepsilon)\right]^2}. \tag{28}$$

After computing the first and second derivatives of $f_N(x)$ in (11), we can rewrite (28) as

$$\mathrm{CRB}_0(\varepsilon) = \frac{\sigma^2}{6\pi^2A^2} \cdot \frac{N^3 \sin^4(\pi\varepsilon/N) p_N(\varepsilon)}{\left[\sin^2(\pi\varepsilon) - N^2 \sin^2(\pi\varepsilon/N)\right]^2} \tag{29}$$

where $p_N(\varepsilon)$ is given by

$$p_N(\varepsilon) = 3\left[N\cos(\pi\varepsilon)\sin(\pi\varepsilon/N) - \sin(\pi\varepsilon)\cos(\pi\varepsilon/N)\right]^2 + (N^2-1)\sin^2(\pi\varepsilon)\sin^2(\pi\varepsilon/N). \tag{30}$$

The result (29) is an important theoretical outcome, as it provides the best accuracy that any unbiased interpolator of two q-shifted spectral lines can attain for a given value of ε. Observing that $f_N(0) = 1$, $f_N'(0) = 0$ and

$$f_N''(0) = -\frac{\pi^2}{3N^2}(N^2-1) \tag{31}$$

the bound (28) for $\varepsilon = 0$ reduces to

$$\mathrm{CRB}_0(\varepsilon)|_{\varepsilon=0} = \frac{3\sigma^2 N}{2\pi^2 A^2 (N^2-1)} \tag{32}$$

and coincides with the classical CRB shown in (6). This means that choosing $q \to 0$ allows the CCRB to be reached as long as the FFO is zero. For values of ε different from zero, the loss with respect to the CCRB is defined as

$$L_0(\varepsilon) = \frac{\mathrm{CRB}_0(\varepsilon)}{\mathrm{CCRB}} \tag{33}$$

and is found to be

$$L_0(\varepsilon) = \frac{N^2(N^2-1)\sin^4(\pi\varepsilon/N) p_N(\varepsilon)}{9\left[\sin^2(\pi\varepsilon) - N^2\sin^2(\pi\varepsilon/N)\right]^2}. \tag{34}$$

Fig. 2 illustrates $L_0(\varepsilon)$ versus $\varepsilon \in [0, 0.5]$ for $N = 64$. It can be seen that the loss monotonically increases with ε and, as predicted by (32), it totally disappears when ε approaches zero. We may thus conclude that the best accuracy achievable during the first iteration by any unbiased iterative DFT interpolator employing two auxiliary spectral lines is non-uniform over the FFO uncertainty range. In particular, a maximum loss of approximately 1.7 with respect to the CCRB is incurred when $\varepsilon = 0.5$. Results obtained with N ranging from 32 to 1024 are practically the same as those reported in Fig. 2. This means that, in practice, the dependence of $L_0(\varepsilon)$ on N is weak.

D. CRB Analysis for $\varepsilon = 0$

When an iterative DFT interpolator is used for fine frequency tuning, the residual FFO decreases at each iteration, such that at the end of the procedure is expected to approach zero. For this reason, it is interesting to evaluate the bound (24) for $\varepsilon = 0$. Such a bound is plotted in Fig. 1 (normalized to the CCRB) and its analytical expression is now derived as a function of $q \in [0, 0.5]$. Letting $\varepsilon = 0$ into (21)-(23) and observing that function $f_N(x)$ is even, while its derivative $f_N'(q)$ is odd, produces

$$\mathbf{S}^T\mathbf{D}\mathbf{S} = 2(1-\gamma) f_N^2(q) \tag{35}$$

$$\boldsymbol{\alpha}^T\mathbf{D}\boldsymbol{\alpha} = 2(1+\gamma) f_N'^2(q) \tag{36}$$

and, finally, $\mathbf{S}^T\mathbf{D}\boldsymbol{\alpha} = 0$. Substituting these results into (24), we get

$$\text{CRB}(\varepsilon, q)|_{\varepsilon=0} = \frac{\sigma^2(1-\gamma)}{4NA^2 f_N'^2(q)} \tag{37}$$

which can also be rewritten as

$$\text{CRB}(\varepsilon, q)|_{\varepsilon=0} = \frac{\sigma^2 N^2}{8\pi^2 A^2} \frac{[N\sin(2\pi q/N)\csc^2(\pi q) - 2\cot(\pi q)]\tan^3(\pi q/N)}{[N\tan(\pi q/N)\cot(\pi q) - 1]^2}. \tag{38}$$

Such a bound is useful as it provides the best accuracy that any unbiased interpolator of two q-shifted spectral lines can achieve upon convergence. For large data sets, its expression can be simplified by letting $N\sin(2\pi q/N) \to 2\pi q$ and $N\tan(\pi q/N) \to \pi q$ into (38). The resulting asymptotic bound (aCRB) is given by

$$\text{aCRB}(\varepsilon, q)|_{\varepsilon=0} = \frac{\sigma^2 \pi q^3[\pi q \csc^2(\pi q) - \cot(\pi q)]}{4NA^2[\pi q \cot(\pi q) - 1]^2} \tag{39}$$

and coincides with the asymptotic variance of the QSE reported in [24]. Hence, our CRB analysis demonstrates that, at least for $\varepsilon = 0$, the QSE is asymptotically efficient as it attains the bound (39) for any value of q. At the first iteration, however, the FFO is likely to be different from zero and the QSE efficiency is not guaranteed anymore as in such a specific situation no theoretical analysis is provided in [24].

It is also interesting to evaluate the bound (38) for the fractional shift $q = 1/2$ employed by AME1 and AME2 in [19]. This produces

$$\text{CRB}(\varepsilon, q)|_{\varepsilon=0, q=1/2} = \frac{\sigma^2 N^3}{4\pi^2 A^2} \frac{\sin^4(\pi/2N)}{\cos^2(\pi/2N)} \tag{40}$$

and the corresponding loss with respect to the CCRB is found to be

$$L(\varepsilon, q)|_{\varepsilon=0, q=1/2} = \frac{N^2(N^2-1)\sin^4(\pi/2N)}{6\cos^2(\pi/2N)}. \tag{41}$$

For large data sets, the loss is asymptotically expressed by

$$\lim_{N\to\infty} L(\varepsilon, q)|_{\varepsilon=0, q=1/2} = \frac{\pi^4}{96} \tag{42}$$

which is exactly the same reported in [19]. This means that, for $\varepsilon = 0$ and conditioned to the selected value $q = 0.5$, both AME1 and AME2 are asymptotically efficient as they attain the relevant CRB. Similarly to the QSE, however, their efficiency cannot be validated for other FFO values because theoretical analysis is conducted in [19] only for $\varepsilon = 0$.

IV. Maximum-Likelihood DFT Interpolation

Available interpolation methods for iterative frequency tuning are based on heuristic reasoning and do not obey to any specific optimality criterion. Hence, there is no guarantee that they can operate efficiently at each step of the iterative process. This motivates the search for the ML estimator (MLE) of ε using the observation vector $\mathbf{X}$ expressed in (13). Due to its asymptotic efficiency, for large data records the MLE is expected to provide unbiased FFO estimates with a variance that approaches the bound (24) at any iteration.

A. Derivation of the Concentrated Likelihood Function

In order to derive the MLE, we start from the log-likelihood function (LLF) for the unknown parameters $\{C_R, C_I, \varepsilon\}$. For conciseness, we let $C = C_R + jC_I$ and observe that vector $\mathbf{X}$ is Gaussian distributed with covariance matrix $\mathbf{C}_W$ given in (14) and mean

$$\boldsymbol{\mu} = CN\mathbf{S}(\varepsilon) \tag{43}$$

where $\mathbf{S}(\varepsilon) = [S_{-q}(\varepsilon), S_q(\varepsilon)]^T$ is a real-valued vector with entries

$$S_{\mp q}(\varepsilon) = f_N(\varepsilon \pm q). \tag{44}$$

The LLF for the joint estimation of $\boldsymbol{\xi} = \{C, \varepsilon\}$ is thus expressed by

$$\Gamma_1(\tilde{\boldsymbol{\xi}}) = -\ln(\pi^2 \det \mathbf{C}_W) - [\mathbf{X} - \tilde{C}N\mathbf{S}(\tilde{\varepsilon})]^H \mathbf{C}_W^{-1} \times [\mathbf{X} - \tilde{C}N\mathbf{S}(\tilde{\varepsilon})]. \tag{45}$$

Recalling that $\mathbf{C}_W^{-1} = 1/(N\sigma^2)\mathbf{D}$, after skipping irrelevant additive and multiplicative terms independent of $\tilde{\boldsymbol{\xi}}$, we can equivalently replace $\Gamma_1(\tilde{\boldsymbol{\xi}})$ in (45) by

$$\Gamma_2(\tilde{\boldsymbol{\xi}}) = 2\text{Re}\{\tilde{C}^* a(\tilde{\varepsilon})\} - N|\tilde{C}|^2 b(\tilde{\varepsilon}) \tag{46}$$

where we have defined $a(\tilde{\varepsilon}) = \mathbf{S}^T(\tilde{\varepsilon})\mathbf{D}\mathbf{X}$ and $b(\tilde{\varepsilon}) = \mathbf{S}^T(\tilde{\varepsilon})\mathbf{D}\mathbf{S}(\tilde{\varepsilon})$. Our goal is to find the global maximum of $\Gamma_2(\tilde{\boldsymbol{\xi}})$ with respect to $\tilde{\boldsymbol{\xi}}$. For this purpose, we first compute the derivatives of $\Gamma_2(\tilde{\boldsymbol{\xi}})$ with respect to $\tilde{C}_R$ and $\tilde{C}_I$. Putting such derivatives to zero produces the set of equations

$$\begin{cases} 2\text{Re}\{a(\tilde{\varepsilon})\} - 2N\tilde{C}_R b(\tilde{\varepsilon}) = 0 \\ 2\text{Im}\{a(\tilde{\varepsilon})\} - 2N\tilde{C}_I b(\tilde{\varepsilon}) = 0 \end{cases} \tag{47}$$

which is solved by

$$\hat{C}(\tilde{\varepsilon}) = \frac{1}{N}\frac{a(\tilde{\varepsilon})}{b(\tilde{\varepsilon})} \tag{48}$$

where we have borne in mind that $b(\tilde{\varepsilon})$ is real-valued. The solution $\hat{C}(\tilde{\varepsilon})$ is next substituted back into (46) to replace $\tilde{C}$, yielding the *concentrated* LLF for the estimation of ε in the form

$$\Gamma_3(\tilde{\varepsilon}) = \frac{1}{N}\frac{|a(\tilde{\varepsilon})|^2}{b(\tilde{\varepsilon})}. \tag{49}$$

Recalling (20) and (44), we can write $a(\tilde{\varepsilon})$ and $b(\tilde{\varepsilon})$ as

$$a(\tilde{\varepsilon}) = f_N(\tilde{\varepsilon}+q)(X_{-q} - \gamma X_q) + f_N(\tilde{\varepsilon}-q)(X_q - \gamma X_{-q}) \tag{50}$$

$$b(\tilde{\varepsilon}) = f_N^2(\tilde{\varepsilon}+q) - 2\gamma f_N(\tilde{\varepsilon}+q) f_N(\tilde{\varepsilon}-q) + f_N^2(\tilde{\varepsilon}-q) \tag{51}$$

from which it follows that

$$|a(\tilde{\varepsilon})|^2 = r_0 f_N^2(\tilde{\varepsilon}+q) + 2r_1 f_N(\tilde{\varepsilon}+q) f_N(\tilde{\varepsilon}-q) + r_2 f_N^2(\tilde{\varepsilon}-q) \tag{52}$$

where the coefficients

$$r_0 = |X_{-q} - \gamma X_q|^2 \tag{53}$$

$$r_1 = \text{Re}\left\{(X_{-q} - \gamma X_q)(X_q^* - \gamma X_{-q}^*)\right\} \tag{54}$$

$$r_2 = |X_q - \gamma X_{-q}|^2 \tag{55}$$

are independent of $\tilde{\varepsilon}$. Finally, putting (51) and (52) into (49) and skipping an irrelevant factor $1/N$, yields the equivalent concentrated likelihood function

$$\Gamma(\tilde{\varepsilon}) = \frac{r_0 + 2r_1 h_N(\tilde{\varepsilon}, q) + r_2 h_N^2(\tilde{\varepsilon}, q)}{1 - 2\gamma h_N(\tilde{\varepsilon}, q) + h_N^2(\tilde{\varepsilon}, q)} \tag{56}$$

where $h_N(\tilde{\varepsilon}, q)$ is defined as

$$h_N(\tilde{\varepsilon}, q) = \frac{f_N(\tilde{\varepsilon} - q)}{f_N(\tilde{\varepsilon} + q)}. \tag{57}$$

B. Maximization of the Concentrated Likelihood Function

The ML estimate of ε is the value of $\tilde{\varepsilon}$ where $\Gamma(\tilde{\varepsilon})$ achieves its global maximum, i.e.,

$$\hat{\varepsilon}_{ML} = \arg\max_{\tilde{\varepsilon}} \Gamma(\tilde{\varepsilon}). \tag{58}$$

Observing that $\Gamma(\tilde{\varepsilon})$ depends on $\tilde{\varepsilon}$ only through $h_N(\tilde{\varepsilon}, q)$, the maximization in (58) can be performed by letting

$$z = h_N(\tilde{\varepsilon}, q) \tag{59}$$

and looking for the value of z that maximizes the function

$$\Lambda(z) = \frac{r_0 + 2r_1 z + r_2 z^2}{1 - 2\gamma z + z^2}. \tag{60}$$

The estimate $\hat{\varepsilon}_{ML}$ is eventually obtained by inverting (59). Such a procedure requires the computation of the first derivative of $\Lambda(z)$ with respect to z, which is given by

$$\Lambda'(z) = 2\frac{-(r_1 + \gamma r_2)z^2 + (r_2 - r_0)z + r_1 + \gamma r_0}{(1 - 2\gamma z + z^2)^2}. \tag{61}$$

The roots of $\Lambda'(z)$ are next found by putting the numerator of $\Lambda'(z)$ to zero. Bearing in mind (53)-(55), this leads to the following quadratic equation in z

$$a_0 z^2 + a_1 z + a_2 = 0 \tag{62}$$

where the coefficients $\{a_0, a_1, a_2\}$ are given by

$$a_0 = \gamma |X_{-q}|^2 - \mathrm{Re}\{X_q X_{-q}^*\} \tag{63}$$

$$a_1 = |X_q|^2 - |X_{-q}|^2 \tag{64}$$

$$a_2 = \mathrm{Re}\{X_q X_{-q}^*\} - \gamma |X_q|^2 \tag{65}$$

and obey to the following relation

$$a_1 = -\frac{a_0 + a_2}{\gamma}. \tag{66}$$

Hence, we can rewrite the quadratic equation (62) as

$$\gamma a_0 z^2 - (a_0 + a_2)z + \gamma a_2 = 0 \tag{67}$$

and observe that its discriminant $\Delta = \gamma^2(a_0 - a_2)^2 + (1 - \gamma^2)(a_0 + a_2)^2$ is positive for $|\gamma| < 1$. It follows that the roots

$$\{z_1, z_2\} = \frac{1}{2\gamma a_0}(a_0 + a_2 \pm \sqrt{\Delta}) \tag{68}$$

are always real-valued. The study of the sign of $\Lambda'(z)$ indicates that the maximum of $\Lambda(z)$ occurs at

$$\hat{z} = \frac{1}{2\gamma a_0}(a_0 + a_2 - \sqrt{\Delta}) \tag{69}$$

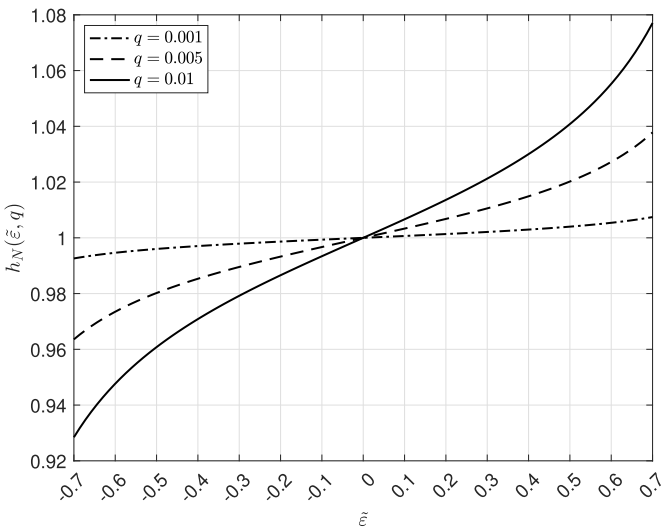

Fig. 3. Function $h_N(\tilde{\varepsilon}, q)$ vs. $\tilde{\varepsilon}$ for $N = 64$ and three different values of q.

irrespective of the sign of a_0. Once $\hat{z}$ has been computed, the ML estimate of ε is found by looking for the value $\hat{\varepsilon}_{ML}$ that satisfies the following relation

$$\hat{z} = h_N(\hat{\varepsilon}_{ML}, q). \tag{70}$$

Since function $h_N(\tilde{\varepsilon}, q)$ cannot be inverted in closed-form with respect to $\tilde{\varepsilon}$, a practical method is now illustrated to get an approximate value of $\hat{\varepsilon}_{ML}$.

C. Computation of the FFO Estimate

Fig. 3 shows the shape of $z = h_N(\tilde{\varepsilon}, q)$ vs. $\tilde{\varepsilon}$ for three different values of q and $N = 64$. As is seen, this function grows monotonically with $\tilde{\varepsilon}$, at least over the considered interval $\tilde{\varepsilon} \in [-0.7, 0.7]$. This fact ensures that equation (70) has a unique solution $\hat{\varepsilon}_{ML}$. The monotonicity of $h_N(\tilde{\varepsilon}, q)$ can be analitically checked by evaluating its derivative with respect to $\tilde{\varepsilon}$. For small values of q, such a derivative is found to be

$$h'_N(\tilde{\varepsilon}, q) \simeq \frac{2\pi^2 q}{N^2 \sin^2(\pi\tilde{\varepsilon}/N)} \frac{1 - f_N^2(\tilde{\varepsilon})}{f_N^2(\tilde{\varepsilon} + q)} \tag{71}$$

from which it follows that $h'_N(\tilde{\varepsilon}, q) \geq 0$ because $f_N^2(\tilde{\varepsilon}) \leq 1$ for any $\tilde{\varepsilon}$. We also observe that, for $N \geq 16$ and $|\tilde{\varepsilon}| \ll N$, the following approximation holds true

$$h_N(\tilde{\varepsilon}, q) \simeq \frac{\mathrm{sinc}(\tilde{\varepsilon} - q)}{\mathrm{sinc}(\tilde{\varepsilon} + q)} \tag{72}$$

where $\mathrm{sinc}(x) = \sin(\pi x)/(\pi x)$. We may thus conclude that $h_N(\tilde{\varepsilon}, q)$ is nearly independent of N. The computation of $\hat{\varepsilon}_{ML}$ in (70) can be performed efficiently through a look-up table (LUT), whose entries are the values $\mathcal{Z} = \{z_k | z_k = h_N(\tilde{\varepsilon}_k, q)\}$ taken by $h_N(\tilde{\varepsilon}, q)$ over an M-point uniform grid $\{\tilde{\varepsilon}_k;\ k = 0, 1, \ldots, M-1\}$. The grid is chosen so as to cover the interval $[-\bar{\varepsilon}, \bar{\varepsilon}]$, where $\bar{\varepsilon}$ is a parameter that must be designed as described shortly. It follows that

$$\tilde{\varepsilon}_k = -\bar{\varepsilon} + k\Delta_M \tag{73}$$

where $\Delta_M = 2\bar{\varepsilon}/(M-1)$ is the quantization step for the variable $\tilde{\varepsilon}$. Hence, letting $z_{\hat{k}}$ and $z_{\hat{k}+1}$ be two consecutive

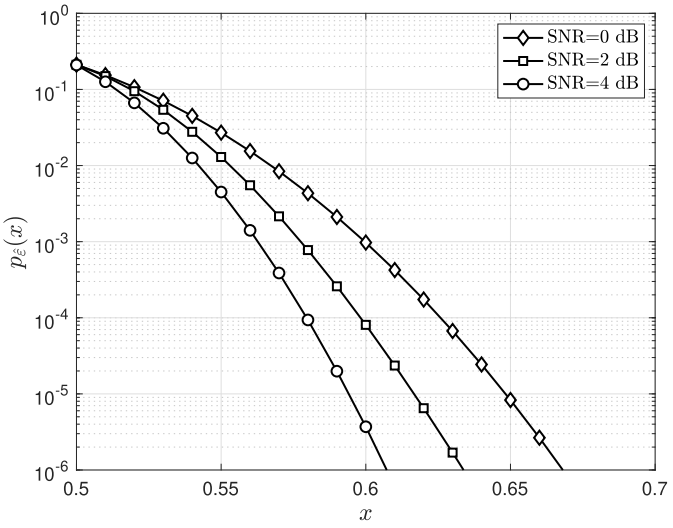

Fig. 4. $p_{\hat{\varepsilon}}(x)$ vs. x with $N = 64$ and ε uniformly distributed in $[0.49, 0.5]$.

entries of $\mathcal{Z}$ such that $z_{\hat{k}} \leq \hat{z} < z_{\hat{k}+1}$, a good approximation of $\hat{\varepsilon}_{ML}$ can be obtained through the following first-order interpolation rule

$$\hat{\varepsilon}_{MLE} = \tilde{\varepsilon}_{\hat{k}} + \frac{\hat{z} - z_{\hat{k}}}{z_{\hat{k}+1} - z_{\hat{k}}} \Delta_M \tag{74}$$

which represents the final FFO estimate provided by MLE.

To avoid large interpolation errors, special care must be taken in the design of $\bar{\varepsilon}$. Recalling that the FFO ε is always less than 0.5 in magnitude, it might seem logical to set $\bar{\varepsilon} = 0.5$. This choice, however, is not recommended. To explain why this is so, we observe that the residual frequency error after running the coarse search is expressed by $\Delta\nu = \nu - \hat{k}_p/N$. Hence, the task of the DFT interpolation stage is to recover the quantity $\varepsilon_{res} = N\Delta\nu = N\nu - \hat{k}_p$ rather than the true FFO value $\varepsilon = N\nu - k_p$. It is worth noting that, as a consequence of possible errors occurring in the IFO estimation process, ε_{res} may occasionally differ from ε. This event is likely to occur whenever the frequency ν is close to the midpoint between two DFT bins, as in this specific situation we may have $\hat{k}_p \neq k_p$ with non-negligible probability. As an example, assume that $k_p = 10$ and $\varepsilon = 0.45$. Then, in the low SNR regime, the IFO estimate may be either $\hat{k}_p = 10$ (corresponding to $\varepsilon_{res} = 0.45$) or $\hat{k}_p = 11$ (corresponding to $\varepsilon_{res} = -0.55$). In the latter case, ε_{res} falls outside the interval $[-0.5, 0.5]$ and the same is expected to occur for its estimate $\hat{\varepsilon}_{MLE} \simeq \varepsilon_{res}$. This fact is substantiated by the results shown in Fig. 4, which illustrates the quantity $p_{\hat{\varepsilon}}(x) = \Pr\{|\hat{\varepsilon}_{MLE}| > x\}$ as a function of $x \in [0.5, 0.7]$ for $N = 64$ and three different SNR values. Here, k_p is fixed to 10, while ε is uniformly distributed within the interval $[0.49, 0.5]$. Furthermore, the LUT cardinality M and the interpolation interval $[-\bar{\varepsilon}, \bar{\varepsilon}]$ are chosen large enough so as to obtain an exact computation of $\hat{\varepsilon}_{ML}$ from (70), i.e., $\hat{\varepsilon}_{MLE} \simeq \hat{\varepsilon}_{ML}$. As is seen, the probability $p_{\hat{\varepsilon}}(x)$ rapidly decreases with x and becomes very small for $x = 0.7$, even at SNR values as low as 0 dB. Accordingly, no performance degradation is expected from the interpolation rule (74) by fixing $\bar{\varepsilon} = 0.7$.

TABLE I
COMPUTATIONAL REQUIREMENTS OF DIFFERENT ESTIMATORS

Estimators	Number of flops	Case study, $N = 64$
MLE	$5N \log_2 N + 16N + 25$	2969
FQE	$5N \log_2 N + 16N + 10$	2954
QSE	$5N \log_2 N + 16N + 8$	2952
AME1	$5N \log_2 N + 16N + 7$	2951
AME2	$5N \log_2 N + 16N + 5$	2949

D. Complexity Analysis

In assessing the processing requirement of MLE, we observe that the N -point DFT operation employed during the initial coarse search needs $(N/2)\log_2 N$ complex products plus $N \log_2 N$ complex additions, while computing the auxiliary DFT coefficients $X_{\pm q}$ requires $2N$ complex products plus $2(N-1)$ complex additions. After evaluating the coefficients a_0 and a_2 through 10 real multiplications plus 6 real additions, additional 5 real products and 3 real additions are required to compute $\hat{z}$ in (69). Finally, we obtain $\hat{\varepsilon}_{MLE}$ in (74) with 3 real products and 2 real additions. The overall number of floating point operations (flops) required by MLE is summarized in the first row of Tab. I for a general value of N (first column) and for $N = 64$ (second column). In writing these quantities, we have borne in mind that a complex product amounts to four real products plus two real additions, while a complex addition is equivalent to two real additions. For comparison, in Tab. I we also report the complexity of FQE, QSE, AME1 and AME2, which provide FFO estimates expressed by

$$\hat{\varepsilon}_{FQE} = \frac{N}{\pi} \arctan\left[\frac{(|X_q| - |X_{-q}|)\sin(\pi q/N)}{(|X_q| + |X_{-q}|)\cos(\pi q/N) - 2|X(\hat{k}_p)|\cos(\pi q)}\right] \tag{75}$$

$$\hat{\varepsilon}_{QSE} = \frac{q\cos^2(\pi q)}{1 - \pi q \cot(\pi q)} \operatorname{Re}\left\{\frac{X_q - X_{-q}}{X_q + X_{-q}}\right\} \tag{76}$$

$$\hat{\varepsilon}_{AME1} = \frac{1}{2}\operatorname{Re}\left\{\frac{X_{0.5} + X_{-0.5}}{X_{0.5} - X_{-0.5}}\right\} \tag{77}$$

$$\hat{\varepsilon}_{AME2} = \frac{1}{2}\frac{|X_{0.5}| - |X_{-0.5}|}{|X_{0.5}| + |X_{-0.5}|}. \tag{78}$$

The results of Tab. I indicate that the processing load of DFT-based interpolation schemes is mostly involved in the computation of the q -shifted spectral lines and in the initial DFT operation, while the final FFO estimate is obtained with negligible additional cost. Consequently, all the considered schemes have practically the same complexity.

V. SIMULATION RESULTS

Computer simulations have been run to assess the performance of MLE and make comparisons with other competing schemes. For the sake of clarity, a description of the main system parameters is provided in Tab. II.

Unless otherwise stated, the number of input data is $N = 64$, while the IFO is fixed to $k_p = 10$. In a first set of simulations, the LUT cardinality M is chosen large

TABLE II
SYSTEM PARAMETERS

Parameter	Description
N	data record length
k_p	integer frequency offset (IFO)
ε	fractional frequency offset (FFO)
Δf	distance between adjacent DFT bins
$\nu = (k_p + \varepsilon)\Delta f$	frequency offset
$f = k_p + \varepsilon$	normalized frequency offset
M	LUT dimension
$[-\bar{\varepsilon}, \bar{\varepsilon}]$	LUT frequency range

enough such that an exact computation of $h_N^{-1}(\hat{z}, q)$ can be assumed in (70), yielding $\hat{\varepsilon}_{MLE} \simeq \hat{\varepsilon}_{ML}$. This allows one to measure the ultimate accuracy achievable by MLE in the absence of any additional error arising from the interpolation rule (74). The impact of M on the system performance is investigated later through a set of dedicated simulations. In any case, parameter $\bar{\varepsilon}$ is fixed to 0.7. We denote by $f = k_p + \varepsilon$ the unknown frequency ν normalized to the distance Δf between two adjacent DFT bins. In all the subsequent experiments, an estimate $\hat{k}_p$ of the IFO is preliminary found through an initial coarse search so as to highlight the threshold effect characterizing the frequency estimation problem. After obtaining $\hat{\varepsilon}$ from the fine interpolation stage, an estimate of f is evaluated as

$$\hat{f} = \hat{k}_p + \hat{\varepsilon}. \tag{79}$$

The accuracy of the investigated FFO estimators is assessed in terms of their mean square error MSE$= \mathrm{E}\{(f - \hat{f})^2\}$ or, alternatively, using the normalized MSE. The latter is a measure of the loss incurred with respect to the CCRB and is expressed by

$$J(\varepsilon, q) = \frac{\mathrm{E}\{(f - \hat{f})^2\}}{\mathrm{CCRB}} \tag{80}$$

where we have explicitly indicated the dependence of J on (ε, q).

Fig. 5 illustrates $J_{MLE}(\varepsilon, q)$ as a function of $\varepsilon \in [0, 0.5]$ for three different values of q and $\mathrm{SNR} = 10$ dB. The normalized CRB $L(\varepsilon, q)$ given in (25) is also shown as a benchmark. As can be seen, MLE attains $L(\varepsilon, q)$ for all values of ε and q as a consequence of its asymptotic efficiency. Although the loss with respect to the CCRB increases with q, letting $q = 0.01$ can provide near optimal performance. This result is in line to the CRB curves shown in Fig. 1, which exhibit a flat profile as long as q is kept small. Accordingly, the value $q = 0.01$ is used in all subsequent simulations.

The impact of the observation length on the performance of MLE is assessed in Fig. 6, where $J_{MLE}(\varepsilon, q)$ is shown as a function of $\varepsilon \in [0, 0.5]$ for $\mathrm{SNR} = 10$ dB and $N = 16, 64$ and 128. It turns out that $J_{MLE}(\varepsilon, q)$ is almost independent of N, at least for $N \geq 16$. In particular, as N increases the normalized MSE approaches the asymptotic value $L_0^{\infty}(\varepsilon) = \lim_{N \to \infty} L_0(\varepsilon)$, with $L_0(\varepsilon)$ as given in (34). Using straightforward calculations, it is found that

$$L_0^{\infty}(\varepsilon) = \frac{3[\pi\varepsilon\cos(\pi\varepsilon) - \sin(\pi\varepsilon)]^2 + [\pi\varepsilon\sin(\pi\varepsilon)]^2}{9[\mathrm{sinc}^2(\varepsilon) - 1]^2}. \tag{81}$$

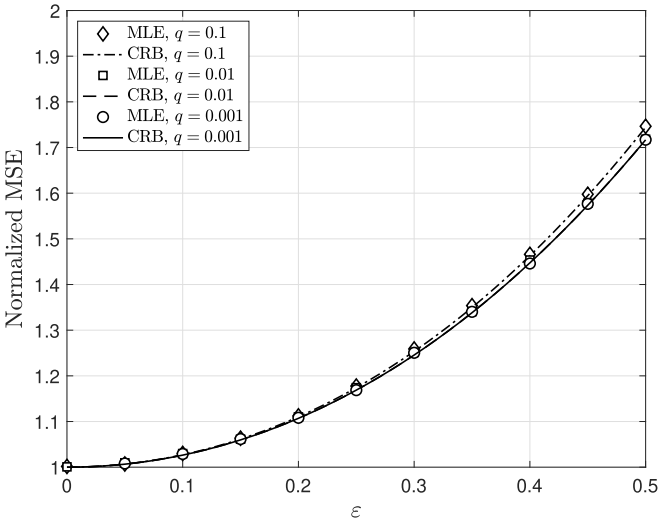

Fig. 5. $J_{MLE}(\varepsilon, q)$ vs. ε for three different values of q.

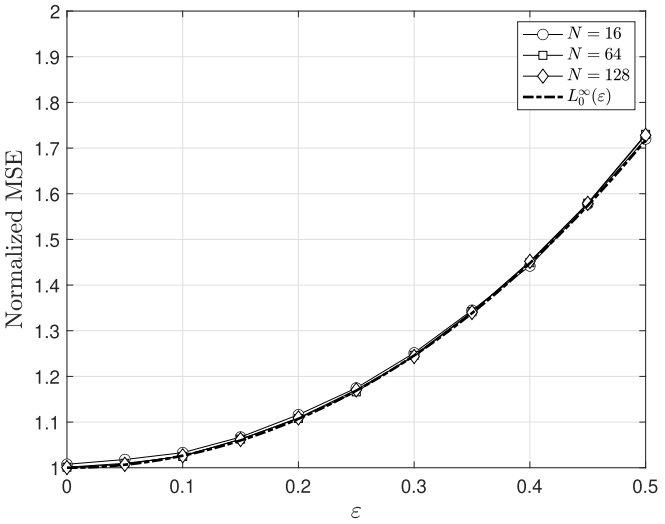

Fig. 6. $J_{MLE}(\varepsilon, q)$ vs. ε for three different values of N and $q = 0.01$.

Fig. 7 compares MLE with other popular competing schemes (FQE, QSE, AME1 and AME2) in terms of normalized MSE vs. ε, measured at $\mathrm{SNR} = 10$ dB. Although all the considered estimators are amenable to iterative implementation, these results have been obtained by performing one single iteration. For small values of ε, the estimators perform satisfactorily and their accuracy is close to the CCRB. As ε increases, however, the estimation accuracy deteriorates and the curves progressively depart from the bound. It is worth noting that, although the loss of MLE with respect to the CCRB is about 1.7 for $\varepsilon = 0.5$, this scheme is still efficient as it attains the bound $\mathrm{CRB}(\varepsilon, q)$ reported in (24) for any value of ε and q. As is seen, FQE and AME1 have similar performance over the entire FFO range and exhibit a maximum loss of 3.2 with respect to the CCRB, which is approximately twice that incurred by MLE. Larger degradations are observed with QSE and AME2. The fact that MLE outperforms the

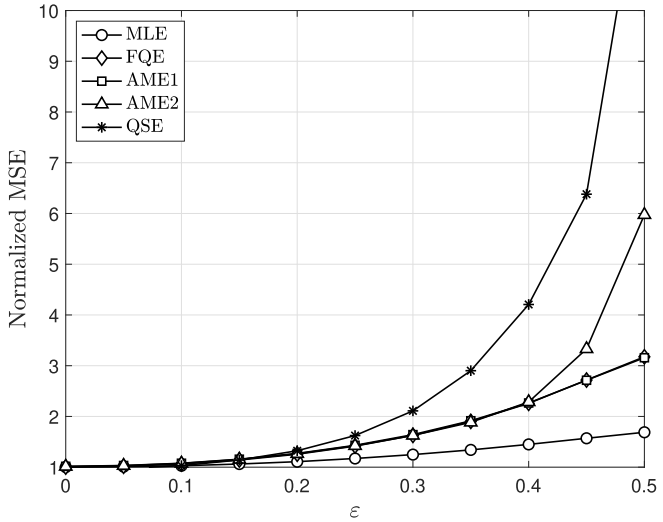

Fig. 7. $J(\varepsilon, q)$ vs. ε for all the considered schemes.

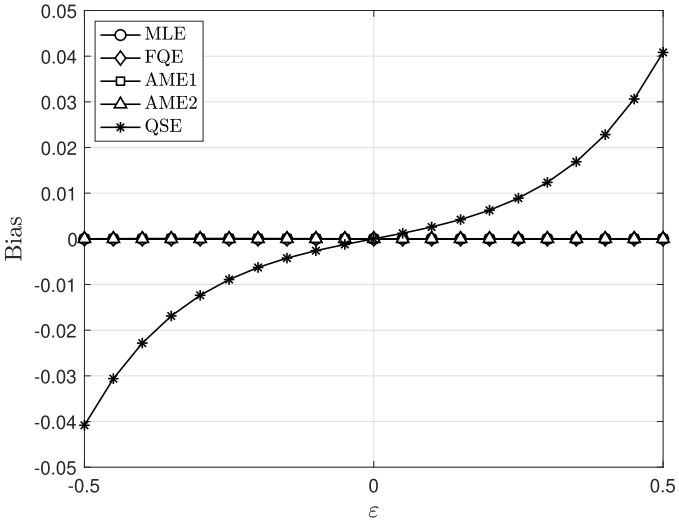

Fig. 9. Bias vs. ε for all the considered schemes.

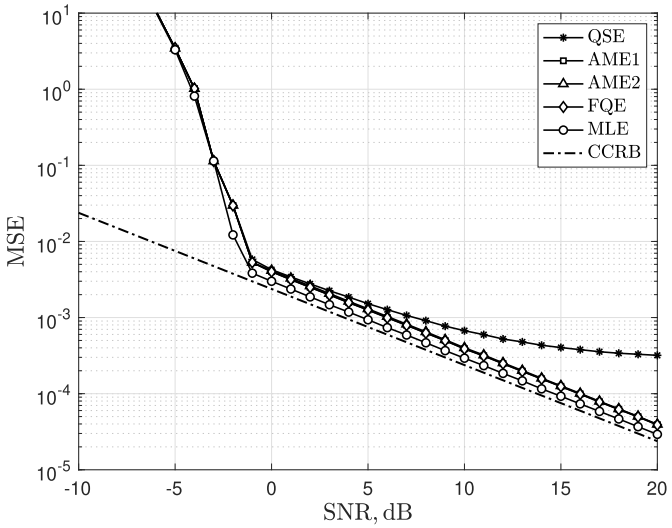

Fig. 8. MSE vs. SNR for all the considered schemes.

other schemes suggests that the latter cannot provide efficient estimates over the full FFO range at their first iteration.

The superiority of MLE over the other estimators is also observed in Fig. 8, where the MSE obtained at the end of the first iteration is plotted as a function of the SNR, with the FFO being uniformly distributed over the range $[-0.5, 0.5)$. In the low SNR regime, the MSE curves are far from the CCRB as a consequence of the threshold phenomenon, which is a manifestation of the occurrence of outliers during the coarse search stage. Since this preliminary stage is common to every DFT interpolation algorithm, the SNR threshold is the same for all the considered schemes. When operating above the threshold, the loss of MLE with respect to the CCRB is less than 1 dB, while it increases to nearly 2.5 dB with FQE, AME1 and AME2, which have comparable performance. At high SNR values, the QSE curve exhibits an irreducible floor, which can be ascribed to a bias affecting the FFO estimate. Such a conjecture is validated by the results shown in Fig. 9, where the bias of all the investigated methods is reported as a function of ε in a noiseless scenario. As is seen, while the other estimators are virtually unbiased, QSE shows a remarkable bias whose absolute value increases with $|\varepsilon|$. The poor performance of QSE after the first iteration is also documented in [24] and has inspired the proposal of the alternative HAQSE method. Indeed, the only difference between HAQSE and QSE is that the former applies the bias-free AME1 before running the QSE iterations in order to get a preliminary reduction of the residual FFO.

In the previous simulations, we showed that the accuracy of the q-shifted DFT interpolators is non uniform over the FFO range $[-0.5, 0.5)$. In order to reduce the impact of ε on the system performance, iterative DFT interpolation can be implemented by repeatedly running MLE or other competing methods. This approach results into a recursive scheme in which, at the ith iteration, two new spectral lines denoted by $X_{-q}^{(i)}$ and $X_{q}^{(i)}$ are computed by applying a shift of $\pm q/N$ to the frequency estimate obtained from the previous step. The residual FFO is then updated by means of the MLE, after replacing $X_{\pm q}$ in (63)-(65) by $X_{\pm q}^{(i)}$. Fig. 10 illustrates the MSE performance of MLE after two iterations and for three different values of N. The FFO is uniformly distributed over $[-0.5, 0.5)$ and the CCRB relative to any considered observation length is also reported for comparison. As can be seen, two iterations are sufficient for MLE to attain the CCRB at SNR values above the threshold. A similar result was also found in [19], [23], and [24] for AME1, AME2, FQE and HAQSE, while at least three iterations are needed with QSE, provided that N is sufficiently large. Indeed, in the presence of short data records, the convergence properties of QSE can be seriously compromized as illustrated in [25].

It is interesting to compare the performance of frequency estimation schemes based on DFT interpolation with alternative approaches that use the sample autocorrelation function of the input data or a subspace decomposition of the observation space. Fig. 11 depicts the MSE vs. SNR obtained with MLE, ESPRIT and the Mengali & Morelli estimator (MME) reported in [7]. The observation length is $N = 64$ and two iterations are performed with MLE. When using the ESPRIT, the

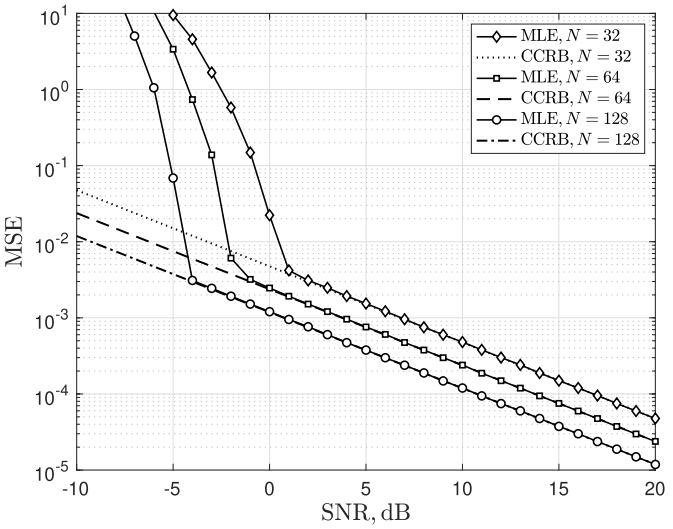

Fig. 10. MSE vs. SNR after two iterations of MLE, for three different values of *N*.

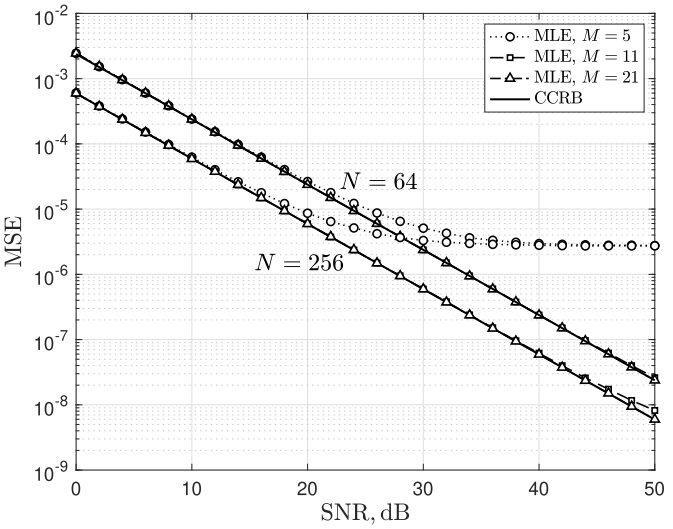

Fig. 12. MSE vs. SNR obtained with MLE for some values of the LUT dimension.

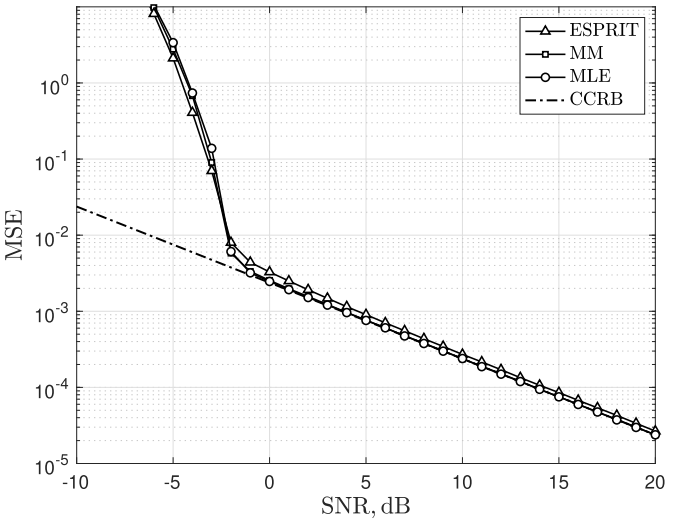

Fig. 11. MSE vs. SNR obtained with MLE, MME and ESPRIT for $N = 64$.

time-domain samples $\{x(n)\}$ are organized into the following snapshot array

$$\mathbf{Y} = \begin{bmatrix} x(0) & x(1) & \cdots & x(N-L) \\ x(1) & x(2) & \dots & x(N-L+1) \\ \vdots & \vdots & \ddots & \vdots \\ x(L-1) & x(L) & \cdots & x(N-1) \end{bmatrix} \tag{82}$$

with L being a suitably designed integer parameter. The frequency estimate is eventually obtained as

$$\hat{f}_{ESPRIT} = \frac{N}{2\pi} \arg \left\{ \sum_{\ell=0}^{L-2} \hat{u}(\ell)\hat{u}(\ell+1) \right\} \tag{83}$$

where $\hat{\mathbf{u}} = [\hat{u}(0), \hat{u}(1), \dots, \hat{u}(L-1)]^T$ is the eigenvector associated with the largest eigenvalue of the sample correlation matrix $\hat{\mathbf{R}} = \mathbf{Y}\mathbf{Y}^H$. In our simulations we use $L = \lfloor N/3 \rfloor$, as this value was found to provide the best MSE performance. The results shown in Fig. 11 indicate that all the considered schemes exhibit the same SNR threshold, which is approximately -2 dB. This corroborates the idea that the threshold phenomenon is not a peculiar feature of the coarse search stage that precedes every DFT interpolation algorithm, but it is rather an unavoidable consequence of the nonlinear nature of the frequency estimation problem. At SNR values above the threshold, MME and MLE perform similarly and attain the CCRB. However, recalling that their complexity is in the order of $\mathcal{O}(N^2)$ and $\mathcal{O}(N \log_2 N)$, respectively, MME is more computationally demanding then MLE. As for the ESPRIT, it requires a complexity as high as $\mathcal{O}(N^3)$, while exhibiting a loss of nearly 0.5 dB with respect to the CCRB. This explains why subspace-based methods are normally employed in the context of multitone parameter estimation, while they are not recommended in the presence of a single sinusoidal signal. It is worth observing that, in principle, DFT-based estimators can be generalized to operate in a multi-component scenario as well. An example is found in [28], where the QSE is used to resolve multiple sinusoids through an estimate-and-subtract strategy.

The simulation results illustrated so far have been obtained by employing a LUT of large cardinality *M*, which corresponds to assuming an exact computation of $\hat{\varepsilon}_{ML}$ from (70). This way, any degradation arising from the use of the interpolation rule described in (74) has been discarded. At this stage, it is useful to assess the impact of parameter M on the MLE performance. In Fig. 12 we plot the MSE vs. SNR obtained after two iterations of MLE with either $N = 64$ or 256. Three different values of *M* are used, namely $M = 5, 11$ and 21. The FFO is uniformly distributed over the interval $[-0.5, 0.5)$ and $\bar{\varepsilon}$ is still fixed to 0.7. As can be seen, for $M = 21$ the estimation accuracy attains the CCRB over the full SNR range $[0, 50]$ dB. A marginal degradation is observed with $M = 11$ in the high SNR region, while an irreducible floor appears in the MSE curves for $M = 5$. The fact that the floor is the same irrespective of the value of N can be explained by recalling that, in all practical situations, the interpolated function $h_N(\tilde{\varepsilon}, q)$

depends weakly on N as specified in (72). Hence, the accuracy of the interpolation rule (74) is only determined by parameter M, while it is virtually independent of N. The results of Fig. 12 indicate that a LUT of cardinality 21 can provide ideal performance at any SNR value of practical interest. We may thus conclude that, in terms of memory requirement, the LUT is typically much less demanding than the coarse search stage, which needs to store the $N-$ dimensional data record $\{x(n)\}$ before running the DFT operation.

VI. Conclusion

We have investigated the problem of fine frequency estimation for a complex exponential signal embedded in white Gaussian noise. The focus was on DFT interpolation schemes amenable to iterative implementation that employ two auxiliary spectral lines symmetrically shifted by a quantity q with respect to the DFT peak. A first contribution of this work is the formulation of the CRB for the considered estimation problem. The bound is found to depend on both the frequency shift q and the FFO ε. Surprisingly, the best accuracy is achieved when q approaches zero, irrespective of the FFO value. We used the CRB to check whether existing frequency recovery methods that operate with two q-shifted spectral lines are efficient or not at their first iteration. Our results indicate that the loss of these schemes with respect to the bound is negligible when ε is small, but becomes substantial when the FFO is close to ± 0.5. This fact prompted us to investigate the ML estimation of ε based on two auxiliary spectral lines, which represents the second contribution of our work. As expected, the resulting ML estimator (MLE) attains the relevant CRB for any value of ε by virtue of its asymptotic efficiency. Compared to alternative DFT interpolators, it performs better without requiring any increase of the computational burden. When implemented recursively, MLE achieves convergence after two iterations as most other competing methods. However, thanks to its improved performance, in some situations the estimation accuracy can be satisfactory just at the end of the first iteration, thereby dispensing from any further iteration. This results into a remarkable advantage whenever frequency estimation must be accomplished fastly and efficiently, in compliance with the time constraints of the system. Examples in this sense are found in voice communications, noise cancellation, tracking of moving radar targets and Doppler shift compensation in medium and low earth orbit satellite communications. In all these applications, performing more iterations may be impractical due to the increased latency arising from the need of recalculating the q-shifted DFT coefficients at each new iteration run.

Future work on this subject may include the extension of MLE to a multi-component scenario, as an alternative to popular subspace-based or atomic norm minimization techniques. In particular, we will check whether the familiar estimate-and-subtract strategy can be adopted to estimate the parameters of multiple sinusoids through a sequential application of MLE.

Appendix A

In this Appendix we evaluate the average power and the covariance of the noise terms $W_{\pm q}$ expressed in (10). It is easily checked that

$$\mathrm{E}\{W_{r_1}W_{r_2}^*\} = e^{j\pi(N-1)(r_1-r_2)/N}\sum_{n=0}^{N-1}\sum_{\ell=0}^{N-1}\mathrm{E}\{w(n)w^*(\ell)\} \times e^{j2\pi[(\ell-n)k_p+(\ell r_2-nr_1)]/N} \quad (84)$$

where $\mathrm{E}\{w(n)w^*(\ell)\} = \sigma^2$ for $n = \ell$ and it is zero otherwise. Hence, we get

$$\mathrm{E}\{W_{r_1}W_{r_2}^*\} = \sigma^2 e^{j\pi(N-1)(r_1-r_2)/N}\sum_{n=0}^{N-1} e^{j2\pi n(r_2-r_1)/N} \quad (85)$$

which can also be rewritten as

$$\mathrm{E}\{W_{r_1}W_{r_2}^*\} = N\sigma^2 f_N(r_1-r_2) \quad (86)$$

with $f_N(x)$ being defined in (11). The result (86) indicates that $\mathrm{E}\{|W_{\pm q}|^2\} = N\sigma^2$ and $\mathrm{E}\{W_{-q}W_q^*\} = N\sigma^2 f_N(2q)$.

Appendix B

In this Appendix we use the Taylor series concept to evaluate the limit of $\mathrm{CRB}(\varepsilon, q)$ when q approaches zero, as specified in (27). We start by expanding $\gamma = f_N(2q)$ as

$$\gamma = 1 + 2f_N''(0)q^2 + o(q^2) \quad (87)$$

where we have borne in mind that $f_N(0) = 1$ and $f_N'(0) = 0$. Then, combining (31) and (87), produces

$$\gamma = 1 - \frac{2\pi^2}{3N^2}(N^2-1)q^2 + o(q^2) \quad (88)$$

from which it follows that

$$1 - \gamma^2 = \frac{4\pi^2}{3N^2}(N^2-1)q^2 + o(q^2). \quad (89)$$

We proceed further by considering the second order expansion of $f_N(\varepsilon \pm q)$ and $f_N'(\varepsilon \pm q)$ around ε, yielding

$$f_N(\varepsilon \pm q) = f_N(\varepsilon) \pm f_N'(\varepsilon)q + \frac{1}{2}f_N''(\varepsilon)q^2 + o(q^2) \quad (90)$$

and

$$f_N'(\varepsilon \pm q) = f_N'(\varepsilon) \pm f_N''(\varepsilon)q + \frac{1}{2}f_N'''(\varepsilon)q^2 + o(q^2) \quad (91)$$

with $f_N'''(x)$ denoting the third derivative of $f_N(x)$. After substitution of (88), (90) and (91) into (21)-(23), we get the identities

$$\mathbf{S}^T\mathbf{D}\mathbf{S} = 4\left[f_N'^2(\varepsilon) + \frac{\pi^2}{3N^2}(N^2-1)f_N^2(\varepsilon)\right]q^2 + o(q^2) \quad (92)$$

$$\boldsymbol{\alpha}^T\mathbf{D}\boldsymbol{\alpha} = 4\left[f_N''^2(\varepsilon) + \frac{\pi^2}{3N^2}(N^2-1)f_N'^2(\varepsilon)\right]q^2 + o(q^2) \quad (93)$$

$$\mathbf{S}^T\mathbf{D}\boldsymbol{\alpha} = 4\left[f_N'(\varepsilon)f_N''(\varepsilon) + \frac{\pi^2}{3N^2}(N^2-1)f_N(\varepsilon)f_N'(\varepsilon)\right] \times q^2 + o(q^2) \quad (94)$$

which lead to the following expression

$$(\mathbf{S}^T\mathbf{D}\mathbf{S})(\boldsymbol{\alpha}^T\mathbf{D}\boldsymbol{\alpha}) - (\mathbf{S}^T\mathbf{D}\boldsymbol{\alpha})^2 = \frac{16\pi^2(N^2-1)}{3N^2} \times \left[f_N(\varepsilon)f_N''(\varepsilon) - f_N'^2(\varepsilon)\right]^2 q^4 + o(q^4). \quad (95)$$

Finally, putting the results (89), (92) and (95) into (24) yields the expression of $\mathrm{CRB}_0(\varepsilon)$ reported in (28).

REFERENCES

[1] U. Mengali and A. N. D'Andrea, *Synchronization Techniques for Digital Receivers*. New York, NY, USA: Plenum, 1995.

[2] Y. Xia, Y. He, K. Wang, W. Pei, Z. Blazic, and D. P. Mandic, "A complex least squares enhanced smart DFT technique for power system frequency estimation," *IEEE Trans. Power Del.*, vol. 32, no. 3, pp. 1270–1278, Jun. 2017.

[3] M. A. Richards, *Fundamentals of Radar Signal Processing*. New York, NY, USA: McGraw-Hill, 2005.

[4] D. C. Rife and R. R. Boorstyn, "Single tone parameter estimation from discrete-time observations," *IEEE Trans. Inf. Theory*, vol. IT-20, no. 5, pp. 591–598, Sep. 1974.

[5] M. P. Fitz, "Further results in the fast estimation of a single frequency," *IEEE Trans. Commun.*, vol. 42, no. 234, pp. 862–864, Feb./Apr. 1994.

[6] M. Luise and R. Reggiannini, "Carrier frequency recovery in all-digital modems for burst-mode transmissions," *IEEE Trans. Commun.*, vol. 43, nos. 2–4, pp. 1169–1178, Feb. 1995.

[7] U. Mengali and M. Morelli, "Data-aided frequency estimation for burst digital transmission," *IEEE Trans. Commun.*, vol. 45, no. 1, pp. 23–25, Jan. 1997.

[8] W. Liao and A. Fannjiang, "MUSIC for single-snapshot spectral estimation: Stability and super-resolution," *Appl. Comput. Harmon. Anal.*, vol. 40, no. 1, pp. 33–67, 2016.

[9] W. Li, W. Liao, and A. Fannjiang, "Super-resolution limit of the ESPRIT algorithm," *IEEE Trans. Inf. Theory*, vol. 66, no. 7, pp. 4593–4608, Jul. 2020.

[10] Q. Li and G. Tang, "Approximate support recovery of atomic line spectral estimation: A tale of resolution and precision," *Appl. Comput. Harmon. Anal.*, vol. 48, no. 3, pp. 891–948, May 2020.

[11] B. G. Quinn, "Estimating frequency by interpolation using Fourier coefficients," *IEEE Trans. Signal Process.*, vol. 42, no. 5, pp. 1264–1268, May 1994.

[12] B. G. Quinn, "Estimation of frequency, amplitude, and phase from the DFT of a time series," *IEEE Trans. Signal Process.*, vol. 45, no. 3, pp. 814–817, Mar. 1997.

[13] C. Candan, "A method for fine resolution frequency estimation from three DFT samples," *IEEE Signal Process. Lett.*, vol. 18, no. 6, pp. 351–354, Jun. 2011.

[14] C. Yang and W. Wei, "A noniterative frequency estimator with rational combination of three spectrum lines," *IEEE Trans. Signal Process.*, vol. 59, no. 10, pp. 5065–5070, Oct. 2011.

[15] C. Candan, "Analysis and further improvement of fine resolution frequency estimation method from three DFT samples," *IEEE Signal Process. Lett.*, vol. 20, no. 9, pp. 913–916, Sep. 2013.

[16] M. D. Macleod, "Fast nearly ML estimation of the parameters of real or complex single tones or resolved multiple tones," *IEEE Trans. Signal Process.*, vol. 46, no. 1, pp. 141–148, Jan. 1998.

[17] U. Orguner and C. Candan, "A fine-resolution frequency estimator using an arbitrary number of DFT coefficients," *Signal Process.*, vol. 105, no. 10, pp. 17–21, Dec. 2014.

[18] M. Morelli, M. Moretti, and A. A. D'Amico, "Single-tone frequency estimation by weighted least-squares interpolation of Fourier coefficients," *IEEE Trans. Commun.*, vol. 70, no. 1, pp. 526–537, Jan. 2022.

[19] E. Aboutanios and B. Mulgrew, "Iterative frequency estimation by interpolation on Fourier coefficients," *IEEE Trans. Signal Process.*, vol. 53, no. 4, pp. 1237–1242, Apr. 2005.

[20] Y. Liu, Z. Nie, Z. Zhao, and Q. H. Liu, "Generalization of iterative Fourier interpolation algorithms for single frequency estimation," *Digit. Signal Process.*, vol. 21, no. 1, pp. 141–149, Jan. 2011.

[21] C. Gong, D. Guo, B. Zhang, and A. Liu, "Improved frequency estimation by interpolated DFT method," in *Proc. Int. Workshop Inf. Electr. Eng. (IWIEE)*, 2012, pp. 4112–4116.

[22] S. F. Minhas and P. Gaydecki, "A non-iterative approach to frequency estimation of a complex exponential in noise by interpolation of Fourier coefficients," in *Proc. 18th Int. Conf. Digit. Signal Process. (DSP)*, Santorini, Greece, Jul. 2013, pp. 1–6.

[23] L. Fan and G. Qi, "Frequency estimator of sinusoid based on interpolation of three DFT spectral lines," *Signal Process.*, vol. 144, pp. 52–60, Mar. 2018.

[24] A. Serbes, "Fast and efficient sinusoidal frequency estimation by using the DFT coefficients," *IEEE Trans. Commun.*, vol. 67, no. 3, pp. 2333–2342, Mar. 2019.

[25] K. Wu, W. Ni, J. Andrew Zhang, R. P. Liu, and Y. Jay Guo, "Refinement of optimal interpolation factor for DFT interpolated frequency estimator," *IEEE Commun. Lett.*, vol. 24, no. 4, pp. 782–786, Apr. 2020.

[26] B. James, B. D. O. Anderson, and R. C. Williamson, "Characterization of threshold for single tone maximum likelihood frequency estimation," *IEEE Trans. Signal Process.*, vol. 43, no. 4, pp. 817–821, Apr. 1995.

[27] S. M. Kay, *Fundamentals of Statistical Signal Processing: Estimation Theory*. Englewood Cliffs, NJ, USA: Prentice-Hall, 1993.

[28] A. Serbes, "Fast and efficient estimation of frequencies," *IEEE Trans. Commun.*, vol. 69, no. 6, pp. 4054–4066, Jun. 2021.

Antonio Alberto D'Amico received the Dr.Ing. degree in electronic engineering and the Ph.D. degree from the University of Pisa, Italy, in 1992 and 1997, respectively. He is currently an Associate Professor with the Department of Information Engineering, University of Pisa. His research interests are in digital communication theory, with emphasis on synchronization algorithms, channel estimation, and detection techniques.

Michele Morelli (Senior Member, IEEE) received the Laurea degree *(cum laude)* in electrical engineering and the Ph.D. degree in telecommunication engineering from the University of Pisa, Italy, in 1991 and 1995, respectively. From 1992 to 1995, he was with the Department of Information Engineering, University of Pisa. In 1996, he joined the Italian National Research Council (CNR), where he was a Research Fellow for five years. Since 2002, he has been with the Department of Information Engineering, University of Pisa, where he is currently a Professor in digital transmissions and telecommunications. His research interests are in the field of digital communications, with emphasis on synchronization methods, equalization schemes, and precoding techniques. He is a member of the Communication Theory Committee and was a co-recipient of the Best Student Paper Award at the IEEE Vehicular Technology Conference VTC in Fall 2006. He has served as an Editor for IEEE TRANSACTIONS ON WIRELESS COMMUNICATIONS from 2007 to 2011, the IEEE WIRELESS COMMUNICATIONS LETTERS from 2011 to 2016, and the IEEE TRANSACTIONS ON COMMUNICATIONS from 2016 to 2018.

Marco Moretti (Member, IEEE) received the degree in electronic engineering from the University of Florence, Florence, Italy, in 1995, and the Ph.D. degree from the Delft University of Technology, Delft, The Netherlands, in 2000. From 2000 to 2003, he was a Senior Researcher with Marconi Mobile. He is currently an Associate Professor with the University of Pisa, Pisa, Italy. His research interests include optimization algorithms and artificial intelligence for wireless communications, synchronization, and channel estimation. He is currently serving as Area Editor for the IEEE TRANSACTIONS ON SIGNAL PROCESSING.